Han *et al. Biochar* (2023) 5:67
https://doi.org/10.1007/s42773-023-00264-4

Biochar

ORIGINAL RESEARCH

Open Access

Enhanced removal of estrogens from simulated wastewater by biochar supported nanoscale zero-valent iron: performance and mechanism

Yuping Han[1,2], Huanhuan Xu[1,2*], Guangzhou Wang[3], Peiyuan Deng[4], Lili Feng[1,2], Yaoshen Fan[3] and Jiaxin Zhang[5]

Abstract

The intensification of estrogen non-point source pollution has drawn global attention due to their contribution to ecological environment problems worldwide, and it is critical to develop effective, economic and eco-friendly methods for reducing estrogens pollution. To address the agglomeration and oxidation of nano zero-valent iron (nZVI), biochar-nanoscale zero-valent iron composite (nZVI-biochar) could be a feasible choice for estrogens removal. This study summarized biochar and nZVI-biochar preparation, characterization, and unusual applications for estrone (E1), 17β-estradiol (E2), and estriol (E3) removal. The properties of biochar and nZVI-biochar in characterization, effects of influencing factors on the removal efficiency, adsorption kinetics, isotherm and thermodynamics were investigated. The experiment results showed that nZVI-biochar exhibited the superior removal performance for estrogens pollutants compared to biochar. Based on the quasi-second-order model, estrogens adsorption kinetics were observed, which supported the mechanism that chemical and physical adsorption existed simultaneously on estrogens removal. The adsorption isotherm of estrogens could be well presented by the Freundlich model and thermodynamics studies explained that nZVI-biochar could spontaneously remove estrogens pollutants and the main mechanisms involved π-π interaction, hydrophobic interaction, hydrogen bonding and degradation through ring rupture. The products analyzed by GC–MS showed that estrogens degradation was primarily attributed to the benzene ring broken, and Fe^{3+} promoted the production of free radicals, which further proved that nZVI-biochar had the excellent adsorption performances. Generally, nZVI-biochar could be employed as a potential material for removing estrogens from wastewater.

Highlights

- Porous and functional nZVI-biochar was prepared and applied for estrogens removal.
- nZVI-biochar exhibited high adsorption capacities to estrogens pollutants due to π–π interaction, hydrophobic interaction and hydrogen bonding.

Handling editor: Bin Gao

*Correspondence:
Huanhuan Xu
huanhuanxu2022@163.com
Full list of author information is available at the end of the article

- The estrogens adsorption process of nZVI-biochar conformed to quasi-second-order kinetics and the Freundlich model.
- The production of free radicals contributed to the degradation of estrogens.

Keywords Biochar supported nanoscale zero-valent iron, Estrogens, Free radicals, Adsorption, Degradation

Graphical Abstract

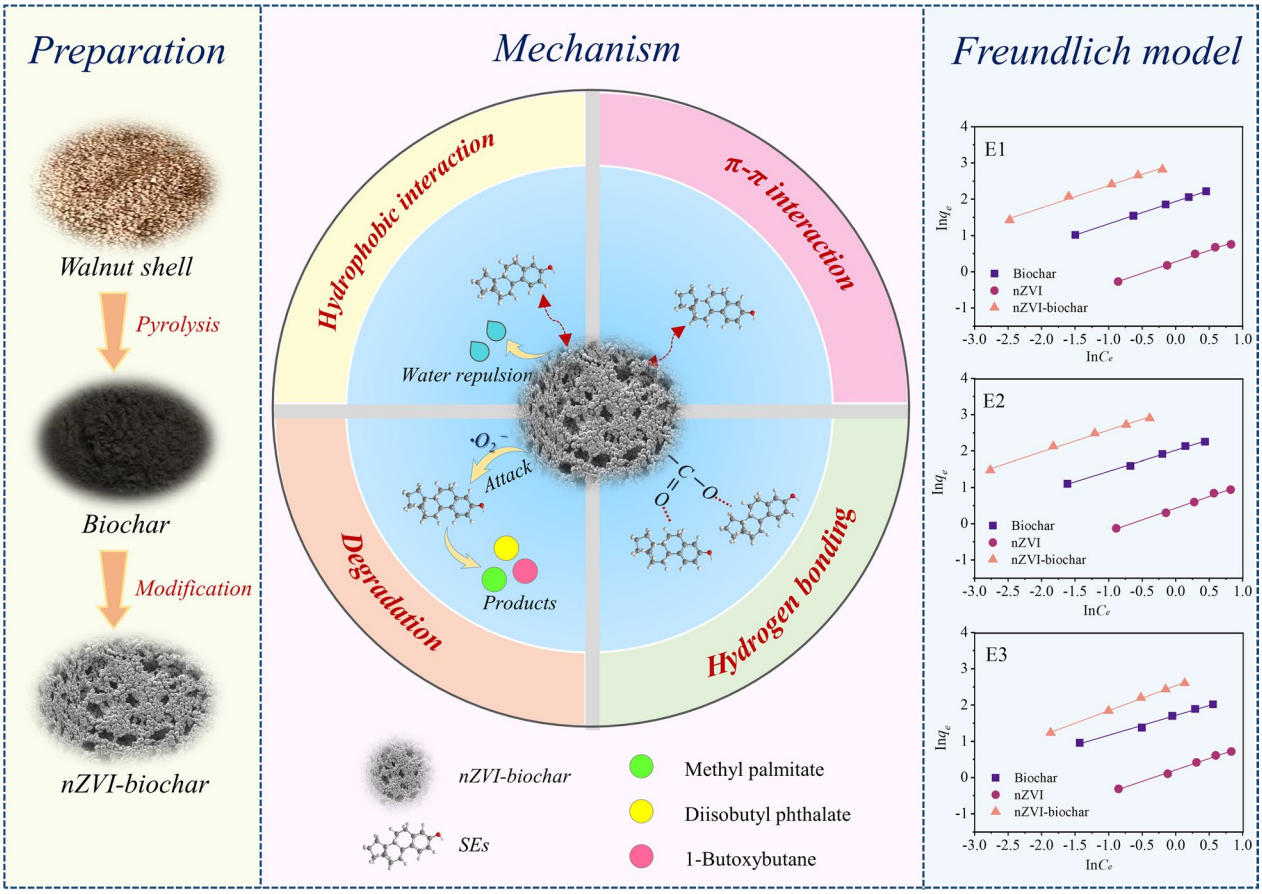

1 Introduction

The increasing of endocrine-disrupting chemicals (EDCs) detected in agricultural, industrial, and domestic sewage is becoming a serious problem threatening human health and ecosystems (Sutherland and Ralph 2019). Compared to other EDCs, E1, E2 and E3 were considered to the most overbearing due to their strong estrogenic activity (Silva et al. 2012), which led to endocrine disorders, abnormalities and dysplasia (Li and Zhang 2014; Hayes et al. 2002; Campbell et al. 2006) at only ng·L^{-1} level. According to previous studies, municipal wastewater was is a hotspot for estrogens, and the presence of E1 and E2 was discovered in sewage treatment plants (STPs) effluent due to the incomplete removal from STPs (Ben et al. 2017). Livestock production and animal waste caused high amounts of estrogens transferred to environment (Adeel et al. 2017). As reported, up to roughly 17,000 μg of estrone (E1) and 384 μg of estradiol (E2) from farm animals per day were released to environment (Matthiessen et al. 2006). Alarmingly, estrogens were even detected in drinking water treatment plants, which meant estrogens posed a serious threat to human health (Deich et al. 2021). Recently, the maximum limit of E2 in water has been set by the European Union to be 0.4 ng·L^{-1} as the Environment Quality Standard.

To reduce estrogens pollution in the environment, various methods were explored to remove estrogens, such as adsorption (Rovani et al. 2016), membrane filtration (Fang et al. 2017), biodegradation (Lucas and Jones 2006), and advanced oxidation processes (Ren et al. 2017). A novel iron-doped graphitic biochar based AOPs was applied to remove estrogens in water, where activated persulfate contributing to degradation of estrogens (Zhang et al. 2019). However, strict operational requirements were needed and secondary pollution occurred simultaneously in the environment by AOPs. Membrane filtration was another method to remove estrogens and 100% of estrogens removal were obtained by microporous polyethersulfone hollow fiber membranes (Hu et al. 2003). Nevertheless, filtration devices were easily blocked, which required higher operating cost. Compared to these approaches, adsorption was regarded as an promising method for estrogens removal from aqueous solutions due to its accessibility and high efficiency (Jawad et al. 2022a, 2022b; Abdulhameed et al. 2022; Zain et al. 2023). Many sorbent materials have been reported for estrogens removal from water, including molecularly imprinted polymers (Noir et al. 2007), powdered activated carbon (Paune et al. 1998), and carbon nanotubes (Joseph et al. 2011). However, it has several limitations to be applied on a large scale due to low adsorption capacity, high cost, and difficult regeneration. In this regard, it is necessary to develop an economical and renewable adsorbent with the excellent adsorption performances for removal of estrogens pollutants based on reuse of waste resources (Zhang et al. 2023; Wu et al. 2022; Huang et al. 2023).

Nano-zero-valent iron (nZVI) has gained significant attention as a potential material for environmental remediation, which could give a large number of adhesion sites for pollutants due to their large specific surface area (Zhao et al. 2023). nZVI with a low reduction potential (E^0) and high reactivity could remove various environmental pollutants by reduction and sorption, such as organic contaminants (Kakavandi et al. 2019), and heavy mentals (Liu et al. 2015). However, nZVI particles were known to face challenges in practical applications such as aggregation and oxidation. Aggregation could lead to reduce contact between nZVI particles and pollutants because of its small size and inherent magnetism, limiting the remediation potential of nZVI. And nZVI was easily aged in the environment and easily oxidized to Fe^{2+}/Fe^{3+} in aerobic environments, which greatly reduced its reactivity. For further applications, many researchers developed effective methods of immobilizing nZVI on carriers (biochar, metal oxide, zeolite, etc.) (Li et al. 2018; Pei et al. 2020; Zhang et al. 2020), which enhanced stability and reactivity of nZVI. For example, nZVI was modified with mesoporous activated carbon to absorb bisphenol A rapidly with lower diffusion resistance (Xu et al. 2022a), and zeolite for ammonia–nitrogen ($NH4^+$-N) removal (Eljamal et al. 2022).

Biochar is a low cost and effective carbonaceous material for dispersing and stabilizing nZVI because of its surface charge, porous structures and abundant functional groups (Karunaratne et al. 2022), which is obtained through carbonization of waste biomass in an oxygen-limited environment. Agricultural wastes, crustacean shells and animal feces are common biochar precursor materials (Li et al. 2022; Sun et al. 2022). Up to 1.5 million ton of walnut shell per year by 2020 was produced in China (Zhang et al. 2015), with superior hydrophilicity, high specific surface area (Xu et al. 2021) and wear resistance (Yu et al. 2016), which was considered as an promising raw material of biochar. Combination of biochar and nZVI could effectively protect nZVI from agglomeration and rapid oxidation and increase dispersion on biochar, thus enhance the removal of pollutants (Wang et al. 2019). As reported, nZVI-biochar has been explored for pollutants removal, such as antibiotics (Wei et al. 2019), Cr (VI) (Liu et al. 2022a), and nitro and chlorinated contaminants (Ahmad et al. 2021). However, there were few studies on estrogens removal by nZVI-biochar.

Hence, the purpose of this study was an advanced overview of efficient estrogens removal from simulated wastewater by a magnetic nZVI-biochar composite. The structural properties of nZVI-biochar were investigated through various characterizations (SEM–EDS, TEM, XRD, FTIR, BET). Removal effects of nZVI-biochar on estrogens were systematically studied, including initial pH, reaction temperature, Fe/C ratio, and contact time. In addition, adsorption kinetics, isotherm and thermodynamic were further investigated for better understanding of the adsorption data. The GC–MS was used to monitor degradation products, which better explained estrogens removal pathway and mechanisms. The outcomes of this research would help to select an effective component of nZVI-biochar, which had practical application value for the degradation of estrogen in simulated wastewater.

2 Materials and approaches

2.1 Biochar and nZVI-biochar preparation used in this experiment

Biochar was prepared by slow pyrolysis of the walnut shell under nitrogen protection (Liu et al. 2022b). Walnut shell was chosen as raw material for biochar production, and was ground into smaller than 2 mm powder by a grinder. After washing with deionized water to remove residual sugar, walnut shell powder was dried in an electric blast drying furnace for 12 h at 65 °C. Then, the feedstock was

pyrolyzed at 700 ℃ using a glass tube furnace in an oxygen-free environment (BR-12NT-120/300–2, China) for obtaining biochar. The heating rate was 15 ℃·min^{-1}, and the pyrolysis continued for 1 h after reaching 700 ℃.

nZVI-biochar particles were prepared using walnut shell biochar as a carrier. As described in the previous study (Xu et al. 2021), nZVI-biochar could be synthesized by liquid-phase reduction method. 24.88 g $FeSO_4{\cdot}7H_2O$ and 5 g biochar were dissolved in 200 ml ethanol–water (ethanol: water = 1:3, v/v) to prepare nZVI-biochar and stirred continuously for 30 min. Afterward, 50 ml $NaBH_4$ reducing agent was added to the solution at a flow rate of 1.5 mL·min^{-1} under vigorous magnetic stirring (150 rpm) for 1 h to ensure the completion of nZVI growth (Wang et al. 2006; Ghauch et al. 2009). Filtered nZVI-biochar was rinsed three times alternately with ethanol and degassed reverse osmosis water (Wang et al. 2006) to avoid nZVI oxidation. This synthesis procedure was conducted by nitrogen continuously bubbled into the reaction system. The obtained samples were dried overnight in a vacuum at 70 ℃ (Sun et al. 2006; Lv et al. 2011).

2.2 Reagents

nZVI-biochar was prepared using $FeSO_4{\cdot}7H_2O$, $NaBH_4$, and ethanol (99%, v/v), all from Shanghai MACKLIN Reagent Co. Ltd. Estrone, 17β-estradiol, and estriol used in the adsorption experiment were purchased from Sigma Aldrich (USA), and the purity was greater than 98%. All organic solvents adopted for high-performance liquid chromatography came from American Tedia company. The compound was dissolved in methanol to prepare a target estrogen and internal standard with a concentration of 1000 mg·L^{-1}, and stored in refrigerator at 4℃. The Wahaha (China) company provided distilled water.

2.3 Characterization of materials

The configuration of different materials was observed by scanning electron microscopy (SEM–EDS, Inspect F50, USA) and transmission electron microscopy (TEM, technai G2 F20, USA). The BET specific surface area and pore size distribution of different materials were determined using a static N_2 adsorption instrument (Autosorb-iQ2-MP, USA). XRD (Smartlab9, Japan) was used to analyze the crystal structure and crystallinity of different materials. NICOLET-380 FTIR spectrometer (USA) was used to record Fourier transform infrared (FTIR) spectra in the range of 4000 to 400 cm^{-1} using KBr disk.

2.4 Sorption experiments

All estrogens removal experiments were accomplished in conical flasks, and 100 mg·L^{-1} NaN_3 was added to restrain microbial degradation. The reaction mediums were stirred with a temperature-controlled water bath oscillator (SHA-B) at 180 rpm to maintain the adsorbent uniformly dispersed in the water environment water environment. To remove oxygen from all the solutions, nitrogen was injected for 15 min. Unless otherwise required, the reaction temperature was room temperature. The initial pH of the solution was adjusted through the addition of 0.1 mol·L^{-1} HCl or 0.1 mol·L^{-1} NaOH. nZVI-biochar was prepared using various mixing ratios of nZVI to biochar (1:1; 2:1; 3:1) in the tests for finding the optimum addition ratios of nZVI to biochar. The adsorption study was conducted with different materials, pH variations (4 ~ 9), different estrogen concentrations (500, 1000, 1500, 2000, 2500 μg·L^{-1}), different iron-carbon ratios (1:1; 2:1; 3:1), and different temperatures (279, 284, 298, 324, 349 K). A 0.22 μm membrane was used to filter 1 mL of samples periodically during batch experiments for analysis of estrogens. Each experiment was conducted in triplicate .

The adsorption kinetics of estrogens was studied at 25 ℃. The different absorbents were added alone to investigate the adsorption of estrogens. Three estrogens were initially added to the water solution at an initial concentration of 1000 μg·L^{-1}. All the flasks were stirred at 180 rpm in the dark. Water samples were extracted after 10, 30, 60, 120, 360, 480, and 720 min of shaking, and immediately filtered through a 0.22 μm membrane for estrogens analysis. Each experiment was conducted in triplicate.

Adsorption isotherms and adsorption kinetics were performed under the same conditions. After adding different concentrations of estrogen solution (500 ~ 2500 μg·L^{-1}), all the flasks were stirred at 180 rpm in the dark and sampled after 1 h based on the kinetics results. The samples were immediately filtered through a 0.22 μm membrane for further analysis, and all experiments were conducted in triplicate. The estrogens adsorption by glassware and soluble organic matter, and photodegradation were regarded to be minimal.

2.5 Determination of estrogens concentration and products

The concentration of estrogens was obtained by High Performance Liquid Chromatography (Ultimate 3000 Series), Thermos C18 column (150 mm*4.6 mm, 5 mm). 0.22 μm hydrophilic polyvinylidene fluoride filter membrane was used first for estrogen filtration before testing samples. The wavelength was 200 nm and the column temperature was 25 °C. The injection volume was 50.0 μL and the flow rate was 1.0 mL·min^{-1}. The mobile phase was 50% acetonitrile and 50% deionized water. The content of estrogens was determined adopting a standard curve featuring the correlation coefficient greater than 0.99.

The degradation products of estrogens were analyzed using Gas Chromatography Mass Spectrometry (GC Varian CP3800/MS Saturn2200, USA), and water samples were extracted by Sep-Pak C18. Firstly, 10 mL deionized water was added to the Sep-Pak C18 small column to remove impurities. Then, the filler was soaked in 10 mL methanol for 5 min. Finally, the column was rinsed 3 times with 15 mL deionized water at a flushing rate of 1–2 mL·min^{-1}. Then 1 L water sample passed through the C18 with a flow rate of 5 mL·min^{-1}. The tested item remained on the C18 small column and was vacuum dried for 5 min to remove any residual moisture. Using a nitrogen blowing instrument, the concentrated pollutant was completed by washing with 10 mL acidified methanol and 20 mL dichloromethane at 1 mL·min^{-1} after 30-min drying at 40 °C, and then transferred to a 1.5 mL injection bottle. Afterward, 50μL of BSTFA and pyridine was added, and the concentrate was derivatized at 70 °C for 45 min and 1 μL was taken for analysis.

2.6 Data analysis

The adsorption kinetics behavior was evaluated by Quasi-first-order (QFO), Quasi-second-order (QSO) kinetics models and Elovich model (Qiu et al. 2009). The results from the adsorption isotherm experiment of different materials were studied adopting Langmuir and Freundlich models. The experiment data were also analyzed with thermodynamic model. The specific formulas and parameters of six models are presented in Table 1.

Where K_1/ (min^{-1}) and K_2/[g (mg·min)$^{-1}$] represent the rate constant of the QFO kinetic model and the QSO kinetic model separately. q_t/ (mg·g^{-1}) is the amount of estrogen adsorbed by different materials at time t, q_e/ (mg·g^{-1}) indicating the equilibrium adsorption capacity. α/ (mg·g^{-1}·h^{-1}) and β/ (g·mg^{-1}) are initial adsorption rate, constants related to surface coverage, respectively. K_F/[mg (g·L)$^{-1}$] and n indicate the Freundlich constant and heterogeneity factor, separately; C_e/ (mg·L^{-1}) represents the equilibrium content of estrogen pollutants, and q_m/ (mg·g^{-1}) and K_L/ (L·mg^{-1}) represent the maximal adsorption capacity and Langmuir binding constant, separately. ΔG (kJ/mol), ΔS/J/ (mol·K), ΔH/ (kJ/mol), K/ (L/g) and T/ (K) represent the Gibbs free energy change, the entropy change, the enthalpy change, the thermodynamic equilibrium constant, and the Kelvin temperature, respectively. R is the ideal gas constant, and R=8.314 J/(mol·L).

Table 1 Formulas and parameters used in kinetics, isotherm and thermodynamic models

Experiment type	Model	Equation
Kinetics	Quasi-first-order	$q_t = q_e(1 - e^{-K_1 t})$
	Quasi-second-order	$q_t = K_2 t q_e^2/(1 - K_2 t q_e)$
	Elovich	$q_t = \ln(\alpha \times \beta)/\beta + \ln t/\beta$
Isotherm	Langmuir	$C_e/q_e = 1/(q_m K_L) + C_e/q_m$
	Freundlich	$\ln q_e = \ln K_F + \ln C_e/n$
Thermodynamic		$\Delta G = -RT \ln K$
		$\ln K = \Delta S/R - \Delta H/RT$

3 Results and discussions

3.1 Materials characteristics

Figure 1A, B, D, E exhibit the SEM images of biochar, and nZVI-biochar particles before and after estrogens adsorption. The experimental results presented that the porosity of biochar was obvious and rich, which provided a favorable possibility for the capture of nZVI in the biochar, and the surface morphology and surface area of biochar did not change significantly after usage for estrogens removal, indicating that biochar might have the potential for recycling (He et al. 2014; Zhang et al. 2010a, 2011). Compared with the unmodified nZVI, nZVI particles got immobilization on the surface or pore of biochar. Obviously, the immobilization of nZVI employing biochar avoided the aggregation of nZVI beneficially to keep their high surface and reactivity. In addition, the aggregation of nZVI disappeared after usage for estrogens removal, indicating that nZVI was involved in the degradation of estrogen pollutants.

The surface element compositions of the biochar and nZVI-biochar were analyzed by EDS spectroscopy. The distribution of elemental C, O, Mg, Si, S, K,Ca was observed from the corresponding SEM–EDS mapping images of biochar (Fig. 1 C), and elemental C and O were the main component elements, mainly from the biochar substrate. Moreover, the peaks of Fe were found from the EDS spectra of nZVI-biochar (Fig. 1F), further confirming the successful attaching of nZVI on biochar. In summary, according to their elemental mapping images, nZVI was evenly distributed on the surface of the biochar, which was in accordance with the results by Karunaratne et al. (2022).

The inside morphology and particle size distribution of the original biochar and nZVI-biochar were studied by transmission electron microscopy (TEM). As shown in Fig. 1G, H, the unique spherical structure of nZVI confirmed its agglomeration tendency. The clear edges and the uneven units of smooth surface of biochar contributed to the loading and aggregation of nZVI. TEM results were consistent with the description of SEM, confirming the successful synthesis of the nZVI-biochar.

The XRD pattern of nZVI-biochar is illustrated in Fig. 1I. The XRD pattern of nZVI-biochar exhibited the apparent peak at 2θ=44.65°, indicating that nZVI

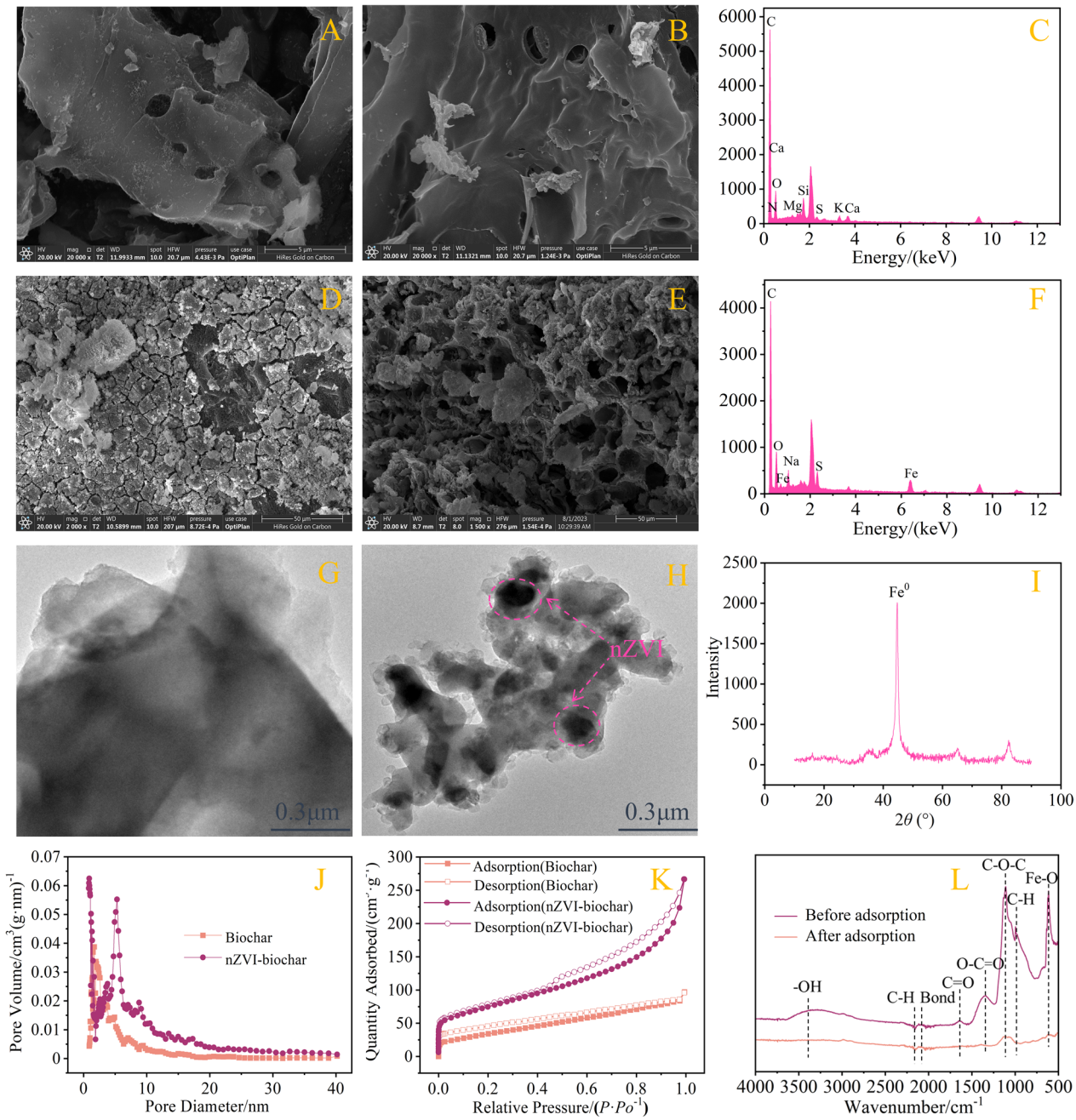

Fig. 1 Materials characteristics. **A**, **B** SEM images of biochar before and after adsorption, **D**, **E** SEM images of biochar before and after adsorption. **C**, **F** SEM–EDS spectra of biochar and nZVI-biochar. **G**, **H** TEM images of biochar and nZVI-biochar. **I** XRD pattern of nZVI-biochar. **J** BET specific surface area and pore volume. **K** N_2 adsorption isotherms. **L** FTIR spectra of nZVI-biochar before and after adsorption

particles were successfully loaded on the surface of biochar (Dai et al. 2016). Furthermore, a weak oxidation peak was detected at $2\theta = 34.65°$, which was assigned to oxidation of nZVI during preparation, drying and storage (Jiang et al. 2011).

The BET specific surface area and pore volume of the nZVI-biochar composites were calculated to be 756.59 $m^2 \cdot g^{-1}$ and 0.47 $cm^3 \cdot g^{-1}$, respectively, much larger than those of biochar (116.87 $m^2 \cdot g^{-1}$ and 0.19 $cm^3 \cdot g^{-1}$) due to the deposition of magnetic nanoparticles on the surface and the macropore's inner wall of biochar, which exposed that nZVI-biochar had more adsorption capacity than biochar. By increasing BET specific surface area and pore volume, nZVI-biochar may have a greater contact

opportunity with estrogens, thus improving estrogens removal efficiency. The aperture distribution and N_2 adsorption/desorption isotherms of biochar and nZVI-biochar are shown in Fig. 1K. The adsorption/desorption isotherms of nZVI-biochar and biochar presented a typical hysteresis loop, indicating the presence of mesopores (Mao et al. 2016), which contributed to the adsorption of estrogens.

Figure 1L shows the FTIR spectra of nZVI-biochar adsorbents before and after estrogens removal. Obvious changes of FTIR band characteristics occurred in nZVI-biochar after interaction with estrogens. Firstly, the band for O–H groups vanished, emphasizing the importance of hydrogen bonding in estrogen adsorption. According to Jia et al. (2020), the hydroxyl groups could act as hydrogen donors, bonding with oxygen atoms from estrogens. Secondly, the intensity of aromatic C-H out-of-plane vibrations was found to be reduced, which indicated that the estrogens–π interaction occurred during estrogens adsorption (Wei et al. 2020). A stable combination of a π from aromatic C–H with another π from estrogens anions could improve the adsorption onto nZVI-biochar. Thirdly, the stretching vibrations of oxygen-containing groups such as C=O and C–O were also weakened with slight shift in peak position, implying that the oxygen containing functional groups on nZVI-biochar also participated in estrogens adsorption via surface complexation reaction (Zhu et al. 2021). Finally, a band wavenumber at 613 cm^{-1} of nZVI-biochar attributed to Fe–O transverse vibration, which confirmed the successful introduction of the Fe^0 (Ji et al. 2022). After the reaction, the stretching vibration of Fe–O band was weakened, which suggested that nZVI participated in the reaction of the estrogens on nZVI-biochar.

3.2 Effects of different influencing factors

Figure 2 shows that nZVI exhibited a certain estrogens removal rate (only 11.9%, 13.5%, 11.1% of E1, E2, E3 were removed after 60 min), which was attributed to oxidation and aggregation of nZVI (Song et al. 2023). Whereas, 46.7%, 49.1%, 39.6% of E1, E2, E3 were removed by biochar alone, mainly due to the adsorption of estrogens by biochar. In contrast, 79.7%, 83.9%, 63.3% of E1, E2, E3 were quickly removed by nZVI-biochar within 10 min, which were significantly higher than the removal rates of biochar alone. Furthermore, the adsorption of E1, E2, and E3 on different absorbent materials occurred rapidly in the first 10 min, and then slowly before reaching adsorption equilibrium within 60 min.

Biochar and nZVI-biochar composites with larger specific surface area could provide more estrogen absorption sites than nZVI alone. In addition, distribution of nZVI particles on the surface or porous structure of biochar made nZVI aggregation highly unlikely, which could offer more active sites than pure nZVI (Luo et al. 2014). When nZVI-biochar was added into the reaction system, the primary cell could be formed spontaneously, which improved the removal efficiency of estrogen pollutants, and meanwhile, inhibited the oxidation of nZVI (Dou et al. 2010; Lv et al. 2014) and improved the stability of nZVI-biochar.

The mass ratio of iron to carbon (Fe/C ratios) was crucial in the synthesis of nZVI-biochar, because the combination of nZVI and biochar could offset their limitations, maintain mutual stability and nZVI dispersion in the removal of pollutants. Proper Fe/C ratios promoted the rational arrangement pattern of nZVI inside or outside the carbon skeleton, which may play a role in the reactivity of nZVI-biochar. The influences of iron-carbon mass ratio (1:1, 2:1, 3:1) on estrogens removal were studied and the results are exhibited in Fig. 3A. In 60 min, the removal rates of E1, E2, E3 were 11.9%, 13.5%, 11.1% by nZVI and 46.7%, 49.1%, 39.6% by biochar alone. The removal rates of E1, E2, E3 increased with increasing iron-carbon mass ratio (60.5%, 71.2%, 48.8% for 1:1 iron-carbon mass ratio, 79.7%, 83.9%, 63.3% for 2:1 iron-carbon mass ratio respectively), which could be attributed to two main aspects. Firstly, the increased adsorption sites

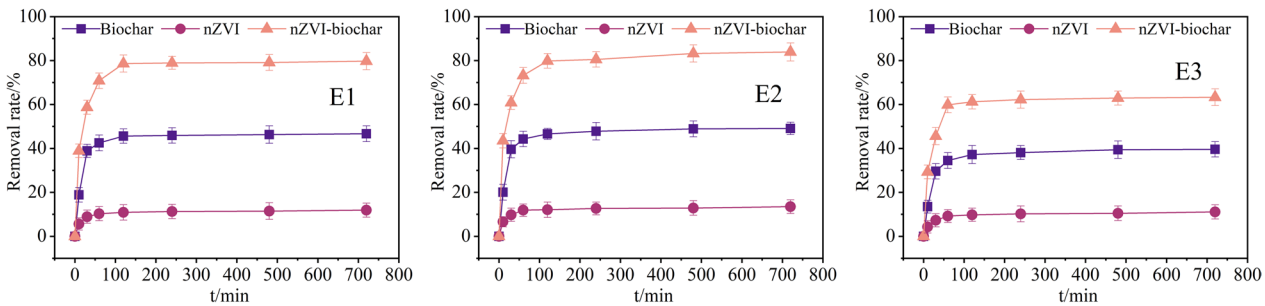

Fig. 2 Effects of removal rate by different materials on estrogens (initial concentration = 1000 μg·L^{-1}, dosage = 0.1 g·L^{-1}, pH = 5.0, T = 25 °C). The values shown in the figure are means ± SD (n = 3)

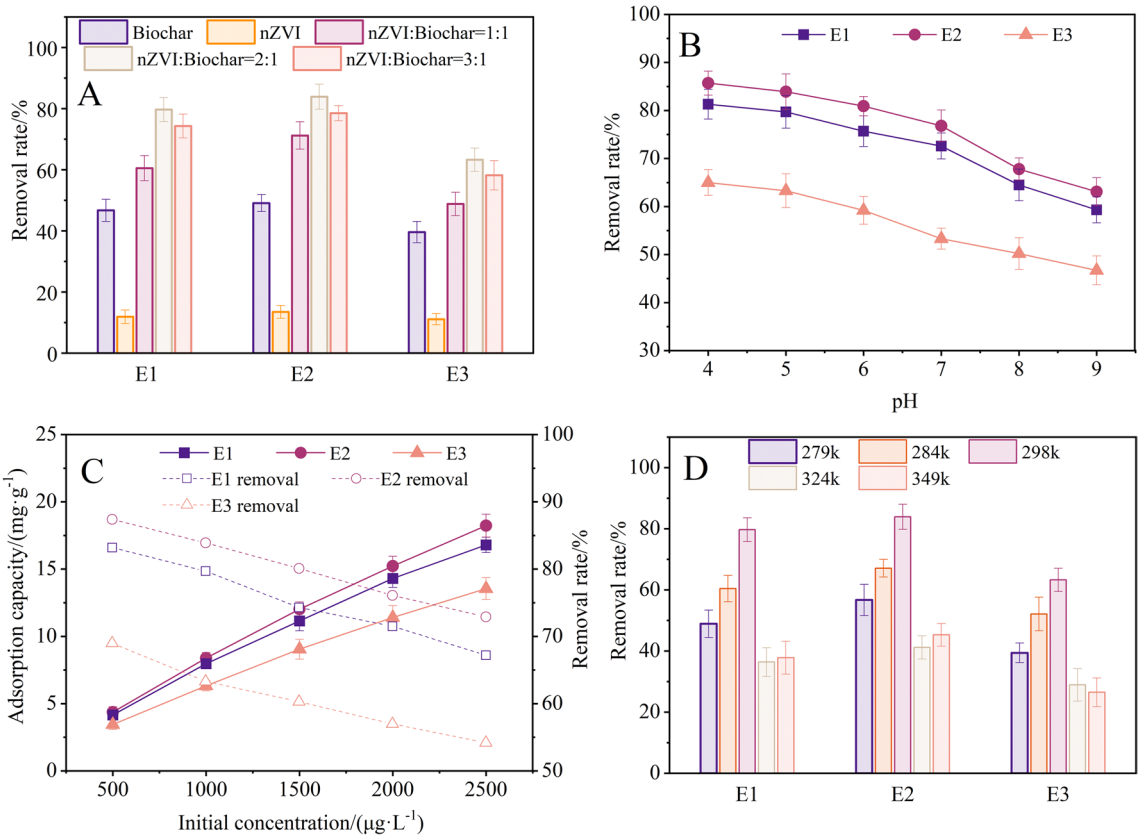

Fig. 3 Effects of different influencing factors. **A** removal rate in different iron-carbon ratio, **B** estrogens removal rates at different pH, **C** initial content effects on estrogen contaminants removal, **D** removal rates of estrogen contaminants at different temperatures. The values shown in the figure are means ± SD (n = 3)

made high availability of the nZVI and estrogens for the reaction, which exhibited better removal performance (Jia et al. 2019). Secondly, the synthesized nZVI-biochar may also acquire substantial galvanic cells with high iron-carbon mass ratio due to the formation of cementite (Wang et al. 2016). However, when the iron-carbon mass ratio was further increased to 3:1, the removal rates of E1, E2, E3 decreased to 74.3%, 78.5%, 58.2%, because nZVI particles distributed on the surface of biochar led to less active sites presented to adsorb estrogen pollutants (Devi and Saroha 2014). Furthermore, a higher dose of nZVI might promote particles agglomeration (Ai et al. 2022), and block reactive sites for contaminants (Zhu et al. 2023) and impede electron transfer, which made a decrease in the removal rate of estrogens. Zhang investigated almost complete removal of CB with nZVI-biochar system, and the mass ratio of 2:1 was conducive to the highest removal rate, indicating that high or low mass ratio of iron to carbon was not suitable for removing CB due to iron's influence on the electron transfer efficiency (Zhang and Wu 2017).

Speciation of the composite and surface charge properties of the adsorbent were affected by the pH of initial solution, and estrogen's pKa value (acid dissociation constant) would affect its ionization state under different pH conditions, which influenced the interaction with adsorbent materials, so pH was the most significant parameter in the adsorption process. Estrogens removal by nZVI-biochar (2:1) at different pH values from 4 to 9 is investigated in Fig. 3B. The outcomes exhibited estrogens removal rate by nZVI-biochar presented little difference at pH 4 and 5. However, the removal rate of estrogens decreased as the solution pH increased from 6 to 9, indicating that acidic conditions were conducive to the highest estrogens removal. This phenomenon may be due to the fact that H^+ could enhance iron oxide corrosion on nZVI surface and suppress nZVI passivation under acidic conditions (Diao et al. 2016), and Fe $(OH)_3$ passivation layers were easily formed on nZVI surface under alkaline conditions, which prevented the contact between nZVI-biochar and estrogens and the electron transfer channel. Additionally, the formation of primary cells between

nZVI and biochar was suffocated (Xie et al. 2017; Lai et al. 2012), resulting in a decreased removal rate of estrogens when the solution pH was greater than 7.

Figure 3C reveals the effects of different initial concentrations of estrogens on the removal rate by 0.1 g·L^{-1} nZVI-biochar composites at the equilibrium time of 60 min. The outcomes exhibited the capacities of E1, E2 and E3 removal were increased by increasing estrogens concentration; and removal rate dropped from 83.2%, 87.4%, 69% to 67.2%, 72.9%, 54.2% as the initial concentration increased from 500 to 2500 μg·L^{-1}, respectively. The similar trend was clearly observed in previously reported studies (Lai et al. 2013; Liu et al. 2013; Xu et al. 2020). Collision times increased with the increase of estrogens concentration, which increased removal rate of estrogens (Wan et al. 2017; Jawad et al. 2022c, 2020). Maintaining the dosage of the nZVI-biochar led to the restricted active adsorption sites on nZVI-biochar, and thereby excessive estrogen was difficult to be completely removed (Jawad et al. 2022c), which meant that the active nZVI-biochar sites to the estrogens pollutants at low concentrations were available.

Temperature held the key to the removal of estrogen pollutants by nZVI-biochar. The removal effects of nZVI-biochar on estrogen pollutants at various temperatures are exhibited in Fig. 3D. Results indicated that 298 K was the optimum temperature for E1, E2, and E3 removal by nZVI-biochar with final removal efficiency of 79.7%, 83.9%, and 63.3%. These results were consistent with previously reported studies, in which the optimum temperature for bisphenol A by NZVI@MAC composites was 298 K (Xu et al. 2022a). Therefore, a cost-effective and eco-friendly material of nZVI-biochar performed excellent potential for practical applications in the wastewater treatment.

3.3 Adsorption kinetics

The kinetic studies gave the equilibrium time and described the removal process, which was an important approach for determining the mechanism. On the basis of previous reports (Maamoun et al. 2018, 2021), the quasi-first-order model (QFO), quasi-second-order (QSO) model, and Elovich model were conducted to test the kinetic data. Table 2 exhibits the calculation

Table 2 Kinetic analysis results of estrogens removal by different materials

Estrogen	Material	QFO model			QSO model			Elovich model		
		q_e/ (mg·g^{-1})	K_1/min^{-1}	R^2	q_e/ (mg·g^{-1})	K_2/[g (mg·min)$^{-1}$]	R^2	α/(mg·g^{-1}·h^{-1})	β/ (g·mg^{-1})	R^2
E1	Biochar	4.591	0.056	0.986	4.871	0.018	0.989	466.070	1.821	0.651
	nZVI	1.123	0.055	0.987	1.192	0.027	0.998	147.694	7.142	0.822
	nZVI-Biochar	7.783	0.059	0.901	8.239	0.009	0.996	1042.07	1.103	0.770
E2	Biochar	4.781	0.060	0.909	5.079	0.033	0.935	501.000	1.724	0.831
	nZVI	1.263	0.055	0.982	1.331	0.077	0.996	200.950	6.896	0.700
	nZVI-Biochar	8.009	0.061	0.976	8.480	0.014	0.998	1410.610	1.101	0.845
E3	Biochar	3.847	0.044	0.905	4.123	0.066	0.912	136.379	1.847	0.905
	nZVI	1.033	0.040	0.985	1.106	0.750	0.998	42.140	7.575	0.985
	nZVI-Biochar	6.210	0.052	0.989	6.568	0.025	0.990	692.250	1.355	0.989

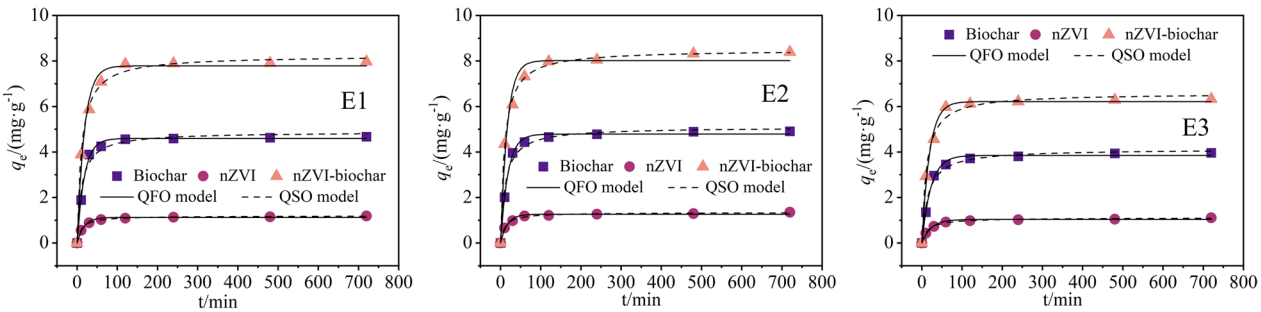

Fig. 4 Adsorption kinetics of E1, E2 and E3 by different materials (initial concentration = 1000 μg·L^{-1}, dosage = 0.1 mg·mL^{-1}, pH = 5, temperature = 25 °C)

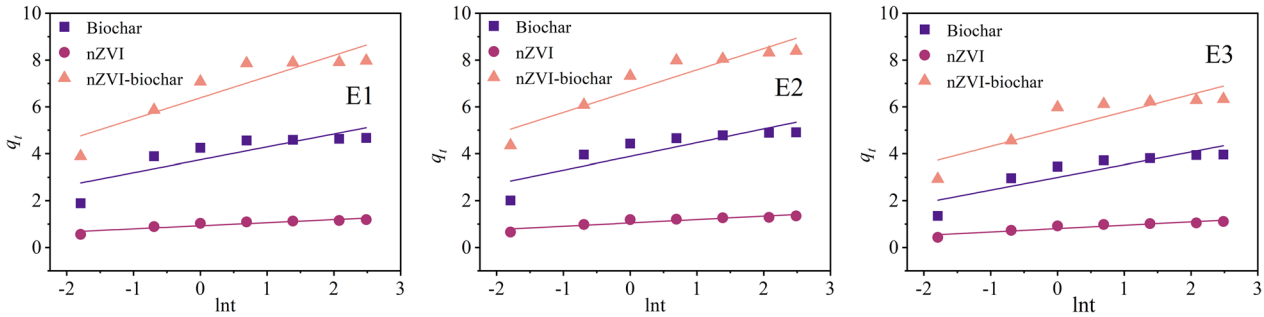

Fig. 5 The Elovich model of E1, E2 and E3 by different materials (initial concentration = 1000 μg·L^{-1}, dosage = 0.1 mg·mL.$^{-1}$, pH = 5 temperature = 25 °C)

parameters of different models. Figures 4 and 5 exhibits the relationships of q_e versus t, q_t versus ln$t$ of estrogens adsorption on biochar, nZVI, and nZVI-biochar, respectively. Compared with the correlation coefficient (R^2) of the QFO model, QSO model and Elovich model, the QSO model was more suitable to characterize the experiment data of estrogens adsorption on nZVI-biochar with the higher R^2 and the closer values of q_e to experimental data. This meant that the adsorption of estrogens was a chemical adsorption (Blázquez et al. 2011; Hameed 2009). The Elovich model was used to describe chemical sorption occurring on a heterogeneous surface (Diagboya et al. 2015). Meanwhile, the Elovich model with a lower R^2 indicated the physical adsorption might involve in the main mechanism. In addition, nZVI-biochar could improve the removal ability in the reduction system of biochar combined with estrogens considering the positive correlation. Table 2 shows that the removal efficiency was in the order of nZVI-biochar > biochar > nZVI.

3.4 Adsorption isotherms

To further investigate the adsorption capacity of biochar, nZVI, and nZVI-biochar, the adsorption isotherms were analyzed using the Langmuir and Freundlich models

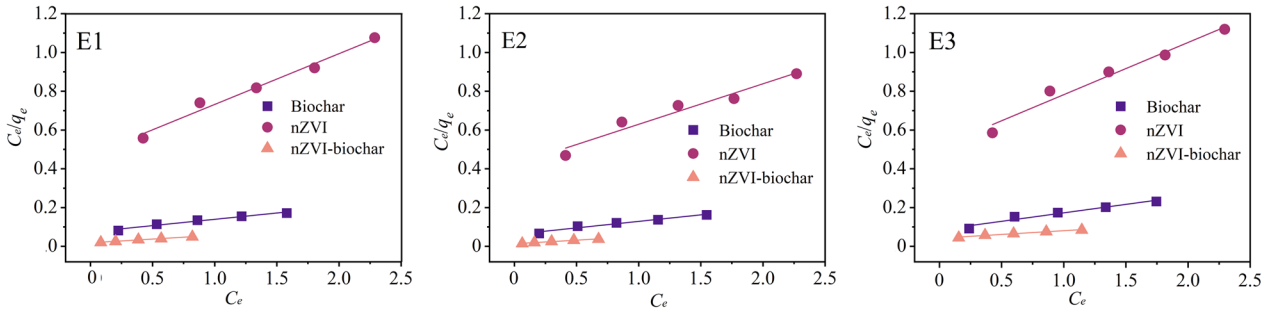

Fig. 6 Langmuir adsorption isotherms of estrogens by different materials

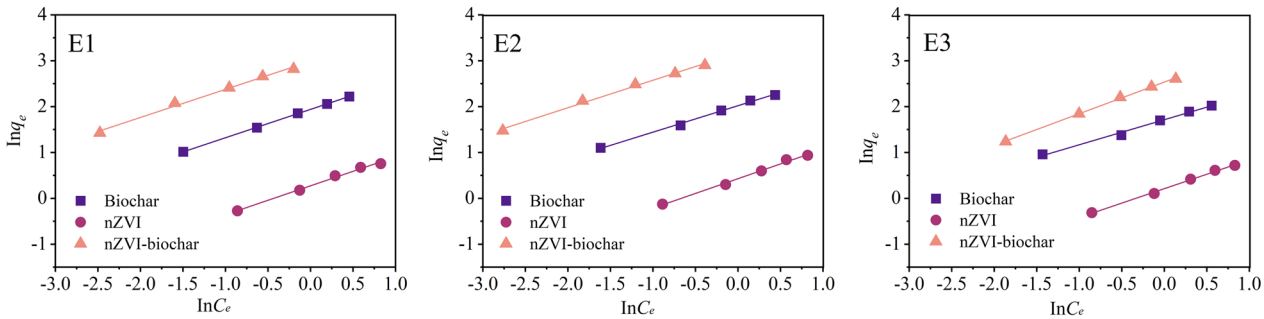

Fig. 7 Freundlich adsorption isotherms of estrogens by different materials

Table 3 Parameters of Langmuir and Freundlich isothermal adsorption models

Estrogen	Material	Langmuir model			Freundlich model		
		q_m/ (mg·g^{-1})	K_L/ (L·mg^{-1})	R^2	K_F/[mg· (g·L)$^{-1}$]	1/n	R^2
E1	Biochar	15.384	0.892	0.963	6.945	0.618	0.999
	nZVI	3.846	0.568	0.978	1.312	0.631	0.996
	nZVI-Biochar	26.315	2.237	0.897	19.826	0.612	0.995
E2	Biochar	14.925	1.098	0.956	7.523	0.576	0.995
	nZVI	4.807	0.495	0.935	1.532	0.643	0.993
	nZVI-Biochar	27.778	2.770	0.988	23.879	0.599	0.994
E3	Biochar	11.494	1.023	0.941	5.545	0.546	0.993
	nZVI	3.717	0.525	0.959	1.232	0.629	0.996
	nZVI-Biochar	25.779	0.932	0.977	12.603	0.689	0.999

under different initial estrogens concentrations ranging from 500 to 2500 μg·L^{-1}. Estrogens adsorption isotherms plots are shown in Figs. 6 and 7, and Table 3 summarizes the fitting equations and parameters. The Langmuir model was adopted for describing the homogeneous adsorption process with a limited number of identical sites, and each adsorbate molecule features a permanent enthalpy and adsorption activation energy (Foo and Hameed 2010). Freundlich model was broadly adopted for multilayer adsorption on heterogeneous surfaces with nonuniform adsorption enthalpy distribution (Ng et al. 2002). Based on the relatively high correlation coefficient R^2 ranging from 0.993 to 0.999 of Freundlich models for different materials, it appeared that the energy distribution in real solid surfaces was not quite uniform and monolayer (Vimonses et al. 2009). The values of K_F meant the maximum adsorption capacities of different materials, with the K_F of biochar and nZVI-biochar much higher than that of nZVI, which indicated that nZVI-biochar had the highest removal ability of estrogen, followed by biochar and nZVI. The high removal ability of nZVI-biochar for estrogens was attributed to its high specific surface (Morawski and Inagaki 1997). Furthermore, compared with the unsupported nZVI particles, the stability and activity of nZVI were improved by employing biochar as a carrier.

3.5 Adsorption thermodynamics

In spite of the lower correlation coefficient of the thermodynamic analysis, the results still could provide key information. Thermodynamic fitting parameters of three materials for estrogens adsorption are shown in Table 4. The negative values of ΔG at all reaction temperatures confirmed that the reactions between estrogen pollutants and adsorptive material were spontaneous and favorable excluding nZVI (Peng et al. 2018). Furthermore, the ΔH with negative values disclosed that the estrogens adsorption was exothermic, which indicated that high temperatures were not required for efficient removal performance consistent with the previously mentioned temperature effect. In general, The theoretical ranges of enthalpy changes (ΔH) corresponding to hydrogen bonding, electrostatic interactions and van der Waals forces are 2 ~ 40, 20 ~ 80 and 4 ~ 10 kJ/mol, respectively (Machado et al.

Table 4 Thermodynamics analysis results of estrogens removal by different materials

Material	Estrogen	ΔG					ΔS	ΔH
		279 K	284 K	298 K	324 K	349 K		
Biochar	E1	− 3.353	− 4.499	− 5.377	− 2.518	− 5.236	− 21.366	− 10.292
	E2	− 3.955	− 4.819	− 5.615	− 3.894	− 6.134	− 9.365	− 7.392
	E3	− 2.485	− 3.667	− 4.658	− 2.434	− 3.721	− 12.703	− 7.025
nZVI	E1	0.588	− 0.086	− 0.744	0.979	1.986	− 24.817	− 7.066
	E2	0.231	− 0.274	− 1.102	0.604	1.151	− 18.158	− 5.451
	E3	1.211	0.173	− 0.055	1.786	2.465	− 27.436	− 7.403
nZVI-biochar	E1	− 5.239	− 6.433	− 9.093	− 4.699	− 5.236	− 17.759	− 11.465
	E2	− 5.966	− 7.119	− 9.794	− 5.244	− 6.134	− 16.212	− 11.822
	E3	− 4.342	− 5.635	− 7.055	− 3.777	− 3.721	− 23.421	− 12.088

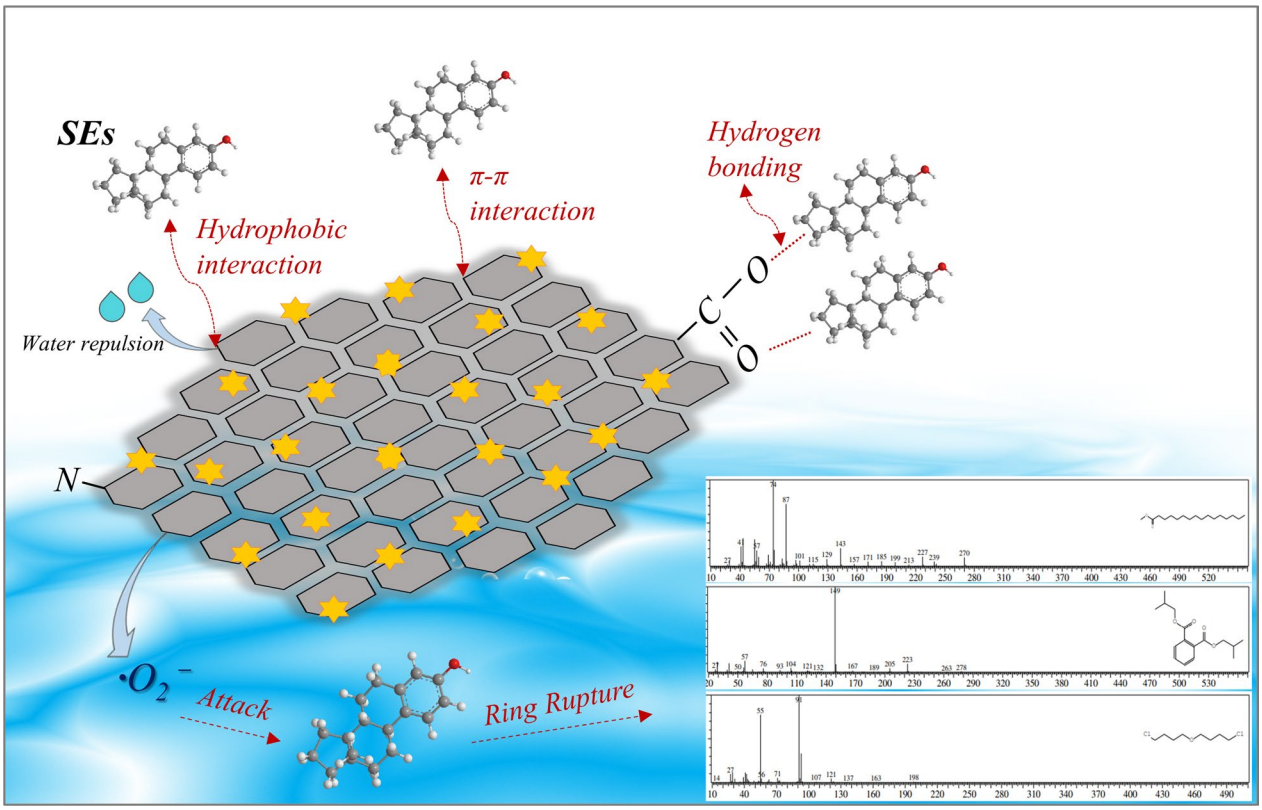

Fig. 8 Degradation of estrogens by nZVI-biochar

2012). Thus, hydrogen bonding and van der Waals forces were the main mechanisms in the adsorption process. In the same temperature, the value of |ΔG| of nZVI-biochar was always higher than that of biochar and nZVI, indicating that nZVI-biochar was more effective for absorbing estrogens. Combined with kinetic studies the results showed that chemical adsorption and physical adsorption existed simultaneously in the process of estrogens adsorption by three materials.

3.6 Adsorption mechanism of estrogens

The mechanism of estrogens removal is primarily based on π–π interaction, hydrophobic interaction, electrostatic interaction and hydrogen bonding among nZVI-biochar and estrogens, and responsible for removal performance (Fig. 8). The higher adsorption capacity of estrogens on nZVI-biochar and biochar confirmed that π–π interaction was of great importance for estrogens removal, which was closely related to the degree of graphitization (Sun et al. 2020). Hydrophobic interaction played an leading role on the adsorption of hydrophobic pollutants (Xie et al. 2020). Hence, the estrogens ($2.6 \leq \log K_{ow} \leq 4$) adsorption on nZVI-biochar was strongly influenced by hydrophobic interactions, and it was an effective adsorbent for removing organic pollutants that were hydrophilic. As reported, the hydrogen bonding was weaken with the increase of solution pH (Zhang et al. 2010b). As pH increased, the removal rate of estrogens decreased slightly, indicating that the strong interaction, hydrophobic interaction and weak hydrogen bonding between estrogens and nZVI-biochar were responsible for the high removal performance. Besides, Xu et al. reported that the oxygen-centered PFRs formed during preparation led to the degradation of estrogens (Xu et al. 2022b). Thereby, the degradation products of estrogens by nZVI-biochar were analyzed by GC–MS. According to the outcomes the degradation of E1, E2 and E3 by nZVI-biochar was mainly through ring rupture and the degradation products were Methyl palmitate, Diisobutyl phthalate, 1-Butoxybutane.

4 Conclusion

In this work, nZVI-biochar was prepared using walnut shell waste as precursor by liquid-phase reduction approach. The results indicated that the dispersion and pore structural parameters were significantly improved compared with nZVI. The adsorption experiments confirmed that nZVI-biochar exhibited good adsorption

performance toward E1, E2, and E3 with the maximum adsorption capacity of 7.97 $mg{\cdot}g^{-1}$, 8.39 $mg{\cdot}g^{-1}$, 6.33 $mg{\cdot}g^{-1}$, respectively. The kinetic fittings suggested that chemical and physical adsorption existed simultaneously on estrogens removal. The isothermal fitting results showed that the adsorption of E1, E2 and E3 occurred as multilayer adsorption on a local non-uniform surface. Combining the characterization results, the adsorption process for E1, E2 and E3 was controlled by various strong–weak interactions including π-π interaction, hydrophobic interaction, hydrogen bonding. In addition, degradation of E1, E2 and E3 by nZVI-biochar was mainly through ring rupture and the degradation products were Methyl palmitate, Diisobutyl phthalate, and 1-Butoxybutane. This study provided a material with excellent adsorption performance for removal of organic pollutants, which realized resource reuse and was in accord with the goal of carbon neutrality.

Acknowledgements
This research has gained support from Study on Colloidal Coagulation and Heavy Metal Adsorption Mechanism of Sediment River (No. 42007158) and Study on the distribution characteristics of birds and the reduction technology of typical pollutants in their habitats in the Yellow River basin (Henan section) (No. 23B180008).

Author contributions
YH: Conceptualization, Resources, Supervision, Writing—Review & Editing. HX (Corresponding Author): Conceptualization, Methodology, Software, Investigation, Formal Analysis, Writing—Original Draft. GW: Data Curation, Visualization, Validation, Investigation. LF: Funding Acquisition, Validation. PD: Resources, Supervision, Funding Acquisition. YF: Software, Resources.

Funding
Study on Colloidal Coagulation and Heavy Metal Adsorption Mechanism of Sediment River (No. 42007158) and Study on the distribution characteristics of birds and the reduction technology of typical pollutants in their habitats in the Yellow River basin (Henan section) (No. 23B180008) supported this research.

Availability of data and materials
Upon reasonable request, the corresponding author would provide the data used or analyzed in the current study.

Declarations

Competing interests
No competing financial interests or personal relationships have been disclosed by the authors that could have affected the work reported here.

Author details
[1]North China University of Water Resources and Electric Power, Zhengzhou 450046, China. [2]Henan Key Laboratory of Water Resources Conservation and Intensive Utilization in the Yellow River Basin, Zhengzhou 450046, People's Republic of China. [3]Yellow River Institute of Hydraulic Research, Yellow River Conservancy Commission, Zhengzhou 450003, Henan Province, China. [4]Zhengzhou Normal University, Zhengzhou 450044, China. [5]State Key Laboratory of Hydrology Water Resources and Hydraulic Engineering, Hohai University, Nanjing 210098, China.

Received: 22 May 2023 Revised: 17 September 2023 Accepted: 22 September 2023
Published online: 23 October 2023

References

Abdulhameed AS, Jawad AH, Ridwan M et al (2022) Chitosan/carbon-doped TiO2 composite for adsorption of two anionic dyes in solution and gaseous SO2 capture: experimental modeling and optimization. J Polym Environ. https://doi.org/10.1007/s10924-022-02532-z
Adeel M, Song X, Wang Y et al (2017) Environmental impact of estrogens on human, animal and plant life: a critical review. Environ Int 99:107–119
Ahmad S, Liu X, Tang J, et al (2022) Biochar-supported nanosized zero-valent iron (nZVI/BC) composites for removal of nitro and chlorinated contaminants. Chem Eng J 431:133187
Ai D, Wei T, Meng Y, et al (2022) Ball milling sulfur-doped nano zero-valent iron@ biochar composite for the efficient removal of phosphorus from water: Performance and mechanisms. Bioresour Technol 357:127316.
Ben W, Zhu B, Yuan X et al (2017) Transformation and fate of natural estrogens and their conjugates in wastewater treatment plants: influence of operational parameters and removal pathways. Water Res 124:244–250
Blázquez G, Martín-Lara MA, Tenorio G et al (2011) Batch biosorption of lead (II) from aqueous solutions by olive tree pruning waste: equilibrium, kinetics and thermodynamic study. Chem Eng J 168(1):170–177
Campbell CG, Borglin SE, Green FB et al (2006) Biologically directed environmental monitoring, fate, and transport of estrogenic endocrine disrupting compounds in water: a review. Chemosphere 65(8):1265–1280
Dai Y, Hu Y, Jiang B et al (2016) Carbothermal synthesis of ordered mesoporous carbon-supported nano zero-valent iron with enhanced stability and activity for hexavalent chromium reduction. J Hazard Mater 309:249–258
Deich C, Kanwischer M, Zhang R, et al (2023) Natural and synthetic estrogenic compounds in the Pearl River Estuary and northern shelf of the South China Sea. Oceanologia 65(1):30–43
Devi P, Saroha AK (2014) Synthesis of the magnetic biochar composites for use as an adsorbent for the removal of pentachlorophenol from the effluent. Bioresour Technol 169:525–531
Diagboya PN, Olu-Owolabi BI, Adebowale KO (2015) Synthesis of covalently bonded graphene oxide–iron magnetic nanoparticles and the kinetics of mercury removal. RSC Adv 5(4):2536–2542
Diao ZH, Xu XR, Chen H et al (2016) Simultaneous removal of Cr (VI) and phenol by persulfate activated with bentonite-supported nanoscale zero-valent iron: reactivity and mechanism. J Hazard Mater 316:186–193
Dou X, Rui L, Bei Z et al (2010) Arsenate removal from water by zero-valent iron/activated carbon galvanic couples. J Hazard Mater 182(1):108–114
Eljamal O, Eljamal R, Maamoun I et al (2022) Efficient treatment of ammonia-nitrogen contaminated waters by nano zero-valent iron/zeolite composite. Chemosphere 287:131990
Fang X, Li J, Li X et al (2017) Internal pore decoration with polydopamine nanoparticle on polymeric ultrafiltration membrane for enhanced heavy metal removal. Chem Eng J 314:38–49
Foo KY, Hameed BH (2010) Insights into the modeling of adsorption isotherm systems. Chem Eng J 156(1):2–10
Ghauch A, Tuqan A, Assi HA (2009) Antibiotic removal from water: elimination of amoxicillin and ampicillin by microscale and nanoscale iron particles. Environ Pollut 157(5):1626–1635
Hameed BH (2009) Spent tea leaves: a new non-conventional and low-cost adsorbent for removal of basic dye from aqueous solutions. J Hazard Mater 161(2–3):753–759
Hayes T, Haston K, Tsui M et al (2002) Herbicides: feminization of male frogs in the wild. Nature 419(6910):895
He F, Zhao D, Roberts C (2014) Stabilization of zero-valent iron nanoparticles for enhanced in situ destruction of chlorinated solvents in soils and groundwater[M]//Nanotechnology Applications for Clean Water. William Andrew Publishing, 2014:491–501
Hu J, Cheng S, Aizawa T et al (2003) Products of aqueous chlorination of 17β-estradiol and their estrogenic activities. Environ Sci Technol 37(24):5665–5670
Huang S, Liu J, Chen S, Wang J, Chen Z, Evrendilek F, Chen T, Huang W, Xie W, Sun S (2023) Converting and valorizing heavy metal-laden post-harvest hyperaccumulator (Pteris vittate L.) into biofuel via acid-pretreated pyrolysis and gasification. Chem Eng J 468:143490
Jawad AH, Hum NNMF, Abdulhameed AS et al (2020) Mesoporous activated carbon from grass waste via H 3 PO 4 -activation for methylene blue dye

removal: modelling, optimisation, and mechanism study. Int J Environ Anal Chem. https://doi.org/10.1080/03067319.2020.1807529
Jawad AH, Abdulhameed AS, Selvasembian R et al (2022a) Magnetic biohybrid chitosan-ethylene glycol diglycidyl ether/magnesium oxide/Fe3O4 nanocomposite for textile dye removal: Box-Behnken design optimization and mechanism study. J Polym Res 29(5):1–15. https://doi.org/10.1007/s10965-022-03067-6
Jawad AH, Rangabhashiyam S, Abdulhameed AS et al (2022b) Process optimization and adsorptive mechanism for reactive blue 19 dye by magnetic crosslinked chitosan/MgO/Fe3O4 biocomposite. J Polym Environ. https://doi.org/10.1007/s10924-022-02382-9
Jawad AH, Saber SEM, Abdulhameed AS et al (2022) Mesoporous activated carbon from mangosteen (Garcinia mangostana) peels by H3PO4 assisted microwave: Optimization, characterization, and adsorption mechanism for methylene blue dye removal. Diamond Related Mater 129:109389
Ji J, Xu S, Ma Z et al (2022) Trivalent antimony removal using carbonaceous nanomaterial loaded with zero-valent bimetal (iron/copper) and their effect on seed growth. Chemosphere. https://doi.org/10.1016/j.chemosphere.2022.134047
Jia T, Zhang B, Huang L et al (2019) Enhanced sequestration of Cr (VI) by copper doped sulfidated zerovalent iron (SZVI-Cu): characterization, performance, and mechanisms. Chem Eng J 366:200–207
Jia X, Zhou J, Liu J et al (2020) The antimony sorption and transport mechanisms in removal experiment by Mn-coated biochar. Sci Total Environ 724:138158. https://doi.org/10.1016/j.scitotenv.2020.138158
Jiang Z, Lv L, Zhang W et al (2011) Nitrate reduction using nanosized zero-valent iron supported by polystyrene resins: role of surface functional groups. Water Res 45(6):2191–2198
Joseph L, Heo J, Park YG et al (2011) Adsorption of bisphenol A and 17α-ethinyl estradiol on single walled carbon nanotubes from seawater and brackish water. Desalination 281(1):68–74
Kakavandi B, Takdastan A, Pourfadakari S et al (2019) Heterogeneous catalytic degradation of organic compounds using nanoscale zero-valent iron supported on kaolinite: mechanism, kinetic and feasibility studies. J Taiwan Inst Chem Eng 96:329–340
Karunaratne TN, Nayanathara RMO, Navarathna CM et al (2022) Pyrolytic synthesis of graphene-encapsulated zero-valent iron nanoparticles supported on biochar for heavy metal removal. Biochar 4(1):1–17. https://doi.org/10.1007/s42773-022-00196-5
Lai B, Zhou Y, Yang P (2012) Passivation of SpongeIron and GAC in Fe0/GAC mixed-potential corrosion reactor. Ind Eng Chem Res 51(22):7777–7785
Lai B, Zhou Y, Yang P et al (2013) Degradation of 3,3′-iminobis-propanenitrile in aqueous solution by Fe0/GAC micro-electrolysis system. Chemosphere 90(4):1470–1477
Li Y, Zhang A (2014) Removal of steroid estrogens from waste activated sludge using Fenton oxidation: influencing factors and degradation intermediates. Chemosphere 105(3):24–30
Li Z, Wang L, Meng J et al (2018) Zeolite-supported nanoscale zero-valent iron: new findings on simultaneous adsorption of Cd (II), Pb (II), and As (III) in aqueous solution and soil. J Hazard Mater 344:1–11
Li S, Shao L, Zhang H et al (2022) A nanoscale observation to explain the discrepancy of electron exchange capacities between biochar containing comparable surface redox-active moieties. Biochar 4(1):1–15. https://doi.org/10.1007/s42773-022-00165-y
Liu M, Xi B, Hou L et al (2013) Magnetic multi-functional nano-fly ash-derived zeolite composites for environmental applications. J Mater Chem A 1(40):12617–12626
Liu T, Wang ZL, Sun Y (2015) Manipulating the morphology of nanoscale zero-valent iron on pumice for removal of heavy metals from wastewater. Chem Eng J 263:55–61
Liu X, Zhang S, Zhang X et al (2022a) A novel lignin hydrogel supported nZVI for efficient removal of Cr (VI). Chemosphere 301:134781
Liu Y, Ma J, Gao J et al (2022b) Stability and interaction of biochar and iron mineral nanoparticles: effect of pH, ionic strength, and dissolved organic matter. Biochar 4(1):1–15. https://doi.org/10.1007/s42773-022-00172-z
Lucas SD, Jones DL (2006) Biodegradation of estrone and 17 β-estradiol in grassland soils amended with animal wastes. Soil Biol Biochem 38(9):2803–2815
Luo J, Song G, Liu J et al (2014) Mechanism of enhanced nitrate reduction via micro-electrolysis at the powdered zero-valent iron/activated carbon interface. J Colloid Interface Sci 435:21–25
Lv X, Xu J, Jiang G et al (2011) Removal of chromium (VI) from wastewater by nanoscale zero-valent iron particles supported on multiwalled carbon nanotubes. Chemosphere 85(7):1204–1209
Lv X, Xue X, Jiang G et al (2014) Nanoscale Zero-Valent Iron (nZVI) assembled on magnetic Fe3O4/graphene for chromium (VI) removal from aqueous solution. J Colloid Interface Sci 417(417):51–59
Maamoun I, Eljamal O, Khalil AME et al (2018) Phosphate removal through nano-zero-valent iron permeable reactive barrier; column experiment and reactive solute transport modeling. Transp Porous Media 125(2):395–412
Maamoun I, Eljamal R, Falyouna O et al (2021) Insights into kinetics, isotherms and thermodynamics of phosphorus sorption onto nanoscale zero-valent iron. J Mol Liq 328:115402
Machado FM, Bergmann CP, Lima EC et al (2012) Adsorption of reactive blue 4 dye from water solutions by carbon nanotubes: experiment and theory. Phys Chem Chem Phys 14(31):11139–11153
Mao HX, Wang SK, Lin JY et al (2016) Modification of a magnetic carbon composite for ciprofloxacin adsorption. J Environ Sci 49:179–188
Matthiessen P, Arnold D, Johnson AC et al (2006) Contamination of headwater streams in the United Kingdom by oestrogenic hormones from livestock farms. Sci Total Environ 367(2–3):616–630
Morawski AW, Inagaki M (1997) Application of modified synthetic carbon for adsorption of trihalomethanes (THMs) from water. Desalination 114(1):23–27
Ng C, Losso JN, Marshall WE et al (2002) Freundlich adsorption isotherms of agricultural by-product-based powdered activated carbons in a geosmin–water system. Bioresour Technol 85(2):131–135
Noir ML, Lepeuple AS, Guieysse B et al (2007) Selective removal of 17-estradiol at trace concentration using a molecularly imprinted polymer. Water Res 41(12):2825–2831
Paune F, Caixach J, Espadaler I et al (1998) Assessment on the removal of organic chemicals from raw and drinking water at a Llobregat river water works plant using GAC. Water Res 32(11):3313–3324
Pei G, Zhu Y, Wen J et al (2020) Vinegar residue supported nanoscale zero-valent iron: remediation of hexavalent chromium in soil. Environ Pollut 256:113407
Peng C, Chai LY, Song YX et al (2018) Thermodynamics, kinetics and mechanism analysis of Cu (II) adsorption by in-situ synthesized struvite crystal. J Central S Univ 25(5):1033–1042
Qiu Y, Zheng Z, Zhou Z et al (2009) Effectiveness and mechanisms of dye adsorption on a straw-based biochar. Biores Technol 100(21):5348–5351
Ren D, Huang B, Yang B et al (2017) Mitigating 17α-ethynylestradiol water contamination through binding and photosensitization by dissolved humic substances. J Hazard Mater 327:197–205
Rovani S, Rodrigues AG, Medeiros LF et al (2016) Synthesis and characterisation of activated carbon from agroindustrial waste—preliminary study of 17β-estradiol removal from aqueous solution. J Environ Chem Eng 4(2):2128–2137
Silva CP, Otero M, Esteves V (2012) Processes for the elimination of estrogenic steroid hormones from water: a review. Environ Pollut 165:38–58
Song H, Liang W, Luo K et al (2023) Simultaneous stabilization of Pb, Cd, and As in soil by rhamnolipid coated sulfidated nano zero-valent iron: Effects and mechanisms. J Hazard Mater 443:130259
Sun Y, Takaoka M, Takeda N et al (2006) Kinetics on the decomposition of polychlorinated biphenyls with activated carbon-supported iron. Chemosphere 65(2):183–189
Sun Z, Zhao L, Liu C et al (2020) Fast adsorption of BPA with high capacity based on π–π electron donor–acceptor and hydrophobicity mechanism using an in-situ sp2 C dominant N-doped carbon. Chem Eng J 381:122510
Sun E, Zhang Y, Xiao Q et al (2022) Formable porous biochar loaded with La-Fe (hydr)oxides/montmorillonite for efficient removal of phosphorus in wastewater: process and mechanisms. Biochar 4(1):1–19. https://doi.org/10.1007/s42773-022-00177-8
Sutherland DL, Ralph PJ (2019) Microalgal bioremediation of emerging contaminants-opportunities and challenges. Water Res 164:114921

Vimonses V, Lei S, Jin B et al (2009) Kinetic study and equilibrium isotherm analysis of Congo Red adsorption by clay materials. Chem Eng J 148(2–3):354–364
Wan C, Ding S, Zhang C et al (2017) Simultaneous recovery of nitrogen and phosphorus from sludge fermentation liquid by zeolite adsorption: mechanism and application. Sep Purif Technol 180:1–12
Wang W, Jin ZH, Li TL et al (2006) Preparation of spherical iron nanoclusters in ethanol-water solution for nitrate removal. Chemosphere 65(8):1396–1404
Wang X, Du Y, Ma J (2016) Novel synthesis of carbon spheres supported nanoscale zero-valent iron for removal of metronidazole. Appl Surf Sci 390:50–59
Wang S, Zhao M, Zhou M et al (2019) Biochar-supported nZVI (nZVI/BC) for contaminant removal from soil and water: a critical review. J Hazard Mater 373:820–834
Wei J, Liu Y, Li J et al (2019) Adsorption and co-adsorption of tetracycline and doxycycline by one-step synthesized iron loaded sludge biochar. Chemosphere 236:124254
Wei D, Li B, Luo L et al (2020) Simultaneous adsorption and oxidation of antimonite onto nano zero-valent iron sludge-based biochar: indispensable role of reactive oxygen species and redox-active moieties. J Hazard Mater 391:122057. https://doi.org/10.1016/j.jhazmat.2020.12205
Wu X, Chen Z, Liu J, Wei Z, Chen Z, Evrendilek F, Sun S, Chen Z (2022) Co-combustion of Zn/Cd-hyperaccumulator and textile dyeing sludge: Heavy metal immobilizations, gas-to-ash behaviors, and their temperature and atmosphere dependencies. Chem Eng J 451:138683
Xie Y, Dong H, Zeng G et al (2017) The comparison of Se (IV) and Se (VI) sequestration by nanoscale zero-valent iron in aqueous solutions: the roles of solution chemistry. J Hazard Mater 338:306
Xie L, Yang D, Lu Q et al (2020) Role of molecular architecture in the modulation of hydrophobic interactions. Curr Opin Colloid Interface Sci 47:58–69
Xu Q, Li W, Ma L et al (2020) Simultaneous removal of ammonia and phosphate using green synthesized iron oxide nanoparticles dispersed onto zeolite. Sci Total Environ 703:135002
Xu L, Su J, Huang T et al (2021) Simultaneous removal of nitrate and diethyl phthalate using a novel sponge–based biocarrier combined modified walnut shell biochar with Fe3O4 in the immobilized bioreactor. J Hazard Mater 414:125578
Xu Q, Liu X, Lai D et al (2022a) One-step synthesis of nanoscale zero-valent iron modified hydrophobic mesoporous activated carbon for efficient removal of bulky organic pollutants. J Clean Prod 356:131854
Xu H, Han Y, Wang G et al (2022b) Walnut shell biochar based sorptive remediation of estrogens polluted simulated wastewater: characterization, adsorption mechanism and degradation by persistent free radicals. Environ Technol Innov 28:102870
Yu Q, Li M, Ji X et al (2016) Characterization and methanol adsorption of walnut-shell activated carbon prepared by KOH activation. J Wuhan Univ Technol Mater. Sci Ed 31(2):260–268
Zain ZM, Abdulhameed AS, Jawad AH et al (2023) A pH-sensitive surface of chitosan/sepiolite clay/algae biocomposite for the removal of malachite green and remazol brilliant blue R dyes: optimization and adsorption mechanism study. J Polym Environ. https://doi.org/10.1007/s10924-022-02614-y
Zhang X, Wu Y (2017) Application of coupled zero-valent iron/biochar system for degradation of chlorobenzene-contaminated groundwater. Water Sci Technol 75(3):571–580
Zhang X, Lin S, Lu XQ et al (2010a) Removal of Pb (II) from water using synthesized kaolin supported nanoscale zero-valent iron. Chem Eng J 163(3):243–248
Zhang S, Shao T, Bekaroglu SSK et al (2010b) Adsorption of synthetic organic chemicals by carbon nanotubes: effects of background solution chemistry. Water Res 44(6):2067–2074
Zhang X, Lin S, Chen Z et al (2011) Kaolinite-supported nanoscale zero-valent iron for removal of Pb2+ from aqueous solution: reactivity, characterization and mechanism. Water Res 45(11):3488
Zhang Y, Yuan S, Wang X et al (2015) Analysis and reflection on development strategy of walnut processing industry in China. Trans Chin Soc Agric Eng 31(21):1–8
Zhang P, Tan X, Liu S et al (2019) Catalytic degradation of estrogen by persulfate activated with iron-doped graphitic biochar: process variables effects and matrix effects. Chem Eng J 378:122141
Zhang Y, Jiao X, Liu N et al (2020) Enhanced removal of aqueous Cr (VI) by a green synthesized nanoscale zero-valent iron supported on oak wood biochar. Chemosphere 245:125542
Zhang J, Chen J, Liu J, Evrendilek F, Zhang G, Chen Z, Huang S, Sun S (2023) Fates of heavy metals, S, and P during co-combustion of textile dyeing sludge and cattle manure. J Clean Prod 383(5):135316
Zhao F, Mu B, Zhang T et al (2023) Synthesis of biochar/clay mineral nanocomposites using oil shale semi-coke waste for removal of organic pollutants. Biochar. https://doi.org/10.1007/s42773-023-00205-1
Zhu G, Lin J, Yuan Q et al (2021) A biochar supported magnetic metal organic framework for the removal of trivalent antimony. Chemosphere 282:131068. https://doi.org/10.1016/j.chemosphere.2021.131068
Zhu L, Chattopadhyay S, Akanbi OE et al (2023) Biochar and zero-valent iron sand filtration simultaneously removes contaminants of emerging concern and Escherichia coliform wastewater effluent. Biochar. https://doi.org/10.1007/s42773-023-00240-y